# Finite momentum superconductivity in superconducting hybrids: Orbital mechanism

M. Yu. Levichev, I. Yu. Pashenkin, N. S. Gusev, and D. Yu. Vodolazov*
*Institute for Physics of Microstructures, Russian Academy of Sciences, 603950 Nizhny Novgorod, GSP-105, Russia*

(Received 31 March 2023; revised 17 September 2023; accepted 18 September 2023; published 26 September 2023)

Normally, in superconductors, as in conductors, in a state with zero current $I$ the momentum of superconducting electrons $\hbar q = 0$. Here we demonstrate theoretically and present experimental evidence that in a superconducting/normal metal (SN) hybrid strip placed in an in-plane magnetic field $B_{\text{in}}$ a finite momentum state ($\hbar q \neq 0$) is realized when $I = 0$. This state is characterized by current-momentum dependence $I(q) \neq -I(-q)$, nonreciprocal kinetic inductance $L_k(I) \neq L_k(-I)$, and different values of depairing currents $I^{\pm}_{\text{dep}}$ flowing along the SN strip in opposite directions. The properties found have *orbital* nature and originate from the density gradient of superconducting electrons $\nabla n$ across the thickness of the SN strip and field-induced Meissner currents. We argue that this type of finite momentum state should be a rather general phenomenon in superconducting structures with artificial or intrinsic inhomogeneities.

DOI: 10.1103/PhysRevB.108.094517

## I. INTRODUCTION

Normally, in superconductors, as in normal conductors (metals or semiconductors), the state with zero total current $I = 0$ is characterized by zero momentum $\hbar q = 0$ of superconducting electrons ($q = \nabla\phi + 2\pi A/\Phi_0$, where $\phi$ is the phase of the superconducting order parameter, $A$ is the vector potential, and $\Phi_0 = \pi\hbar c/|e|$ is the magnetic flux quantum). Such an *ordinary* superconductor has antisymmetric current-momentum dependence $I(q) = -I(-q)$ and symmetric kinetic inductance $L_k(I) = L_k(-I)$ [see Figs. 1(a) and 1(d)]. Kinetic inductance $L_k \sim -dq/dI$ is a measure of inertia of superconducting electrons possessing the kinetic energy $E_k \sim \int n\hbar^2 q^2/(2m)dV \sim \int L_k(I)IdI$ ($m$ is the mass of the superconducting electrons, $n$ is their density, and $V$ is the volume of the superconductor). In superconductors, $L_k$ contributes to the total inductance $L = L_k + L_g$, where $L_g$ is the ordinary (geometric) inductance, which does not depend on $I$.

However, it has been predicted that $q \neq 0$ despite $I$ being equal to 0 for some superconducting systems. The most familiar examples are a ferromagnetic superconductor with magnetic exchange energy of the order of the superconducting gap $\Delta$ and a thin superconducting strip placed in a large in-plane magnetic field $\mu_B B_{\text{in}} \sim \Delta$. In these systems, superconducting pairing occurs with finite center-of-mass momentum of electrons $q_{\text{FF}}$, as has been shown by Fulde and Ferrell [1], due to Zeeman splitting of the energy of electrons having opposite spin. Recently, a similar Fulde-Ferrell (FF) state has been found theoretically in superconductor/ferromagnet (SFM) [2,3], superconductor/ferromagnet/normal metal (SFMN) [4], and nonequilibrium SN hybrids [5–7]. In these hybrid superconductors there are local nonzero currents flowing in opposite directions in different layers, which distinguishes this state from the original FF state. Both cases are referred to here as FF states or superconductors. A FF superconducting strip at $I = 0$ has two degenerate states with $q = \pm q_{\text{FF}}$ due to the finite size effect [8] (for an infinite sample, $q_{\text{FF}}$ may have any direction) and antisymmetric $I(q) = -I(-q)$ dependence [8,9] [see Fig. 1(b)]. At small currents $-I^* < I < I^*$ this system has two stable states [9] which have different values of kinetic inductance $L_k$ [10]; see Fig. 1(e). The depairing current in a FF superconductor does not depend on current direction, which reflects the absence of a particular direction for $q_{\text{FF}}$. As the current increases and approaches $\pm I^*$ [see Fig. 1(b)], the FF superconductor switches to the state having opposite $q_{\text{FF}}$ at $I = 0$. If during this transition the FF superconductor is not heated considerably, it stays in the superconducting state [8].

Besides the FF superconductors, there is another class of superconducting materials where finite momentum superconductivity may exist. These are the so-called noncentrosymmetric (NCS) superconductors, which have no inversion center and where, in the presence of spin-orbit coupling and in-plane magnetic field, finite momentum of superconducting electrons $q_{\text{NCS}}$ with a *particular* direction appears [11–13]. It has been discussed recently that such a NCS superconductor should have different depairing (critical) currents flowing either parallel or antiparallel to $\vec{q}_{\text{NCS}}$ [14–16] and nonreciprocal kinetic inductance $L_k(I) \neq L_k(-I)$ [17] following from the current-momentum dependence $I(q) \neq -I(-q)$ [see Figs. 1(c) and 1(f)]. The difference between critical currents means that ac current with an amplitude between these critical values should produce, in a NCS superconductor, voltage of only one sign. This is the reason why the difference between critical currents is called the superconducting diode effect (SDE).

In this paper we present theoretical and experimental results which demonstrate that finite momentum superconductivity (FMS), typical for the noncentrosymmetric superconductors discussed above, is realized in superconductor/normal metal hybrids *without* spin-orbit coupling in the presence of an in-plane magnetic field [see Fig. 2(a)]. In the SN bilayer there

*vodolazov@ipmras.ru

 

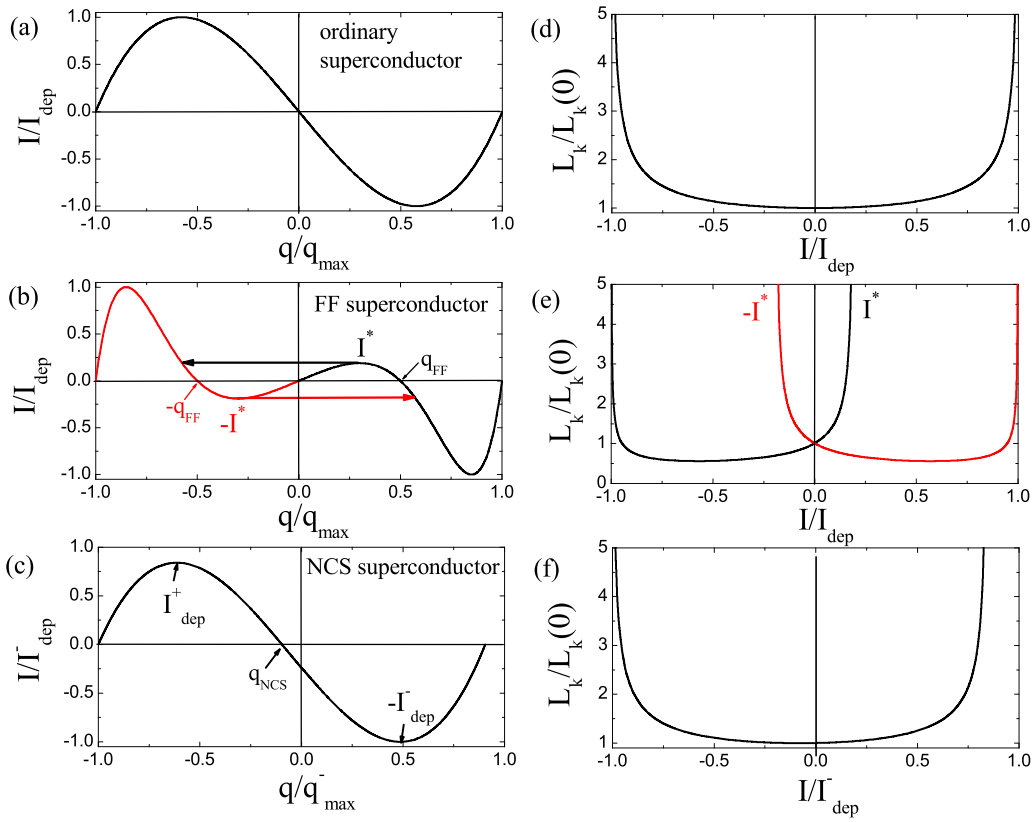


FIG. 1. Current-momentum dependence in ordinary (a), Fulde-Ferrell (b), and noncentrosymmetric (c) thin and narrow superconducting strips with uniform current distribution over the width of the superconductor. In the FF strip, $I(q) = -I(-q)$ (as in an ordinary superconductor), and there are two degenerate finite momentum states ($\pm q_{\rm FF}$), while in the NCS strip $I(q) \neq -I(-q)$ and there is one finite momentum state with $q = q_{\rm NCS}$. In (d)–(f) we present the corresponding dependencies of the kinetic inductance $L_k(I) \sim -dq/dI$. In the NCS superconductor, $L_k(I) \neq L_k(-I)$, which is a fingerprint of this state, as well as the diode effect ($I^-_{\rm dep} \neq I^+_{\rm dep}$). In the ordinary and FF superconductors, $I^-_{\rm dep} = I^+_{\rm dep}$, while $L_k(I)$ is twofold degenerate in the FF superconductor in the current range $-I^* < I < I^*$.

is a thickness-dependent "density" of superconducting electrons $n(z)$ which is a coefficient between the superconducting current density and momentum: $j(z) \sim -|e|n(z)q(z)$. In the normal metal (N) layer, finite $n$ appears due to proximity-induced superconductivity, and usually it is smaller than in the superconductor (S) layer [this case is shown in Fig. 2(b)]. An in-plane magnetic field induces Meissner currents $j(z)$, and superconducting electrons possess momentum $q(z)$. For

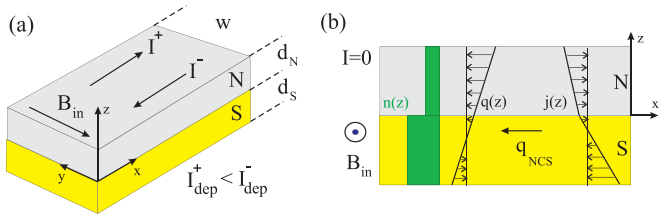


FIG. 2. (a) SN strip with transport currents that have different directions placed in an in-plane magnetic field. (b) Sketch of the thickness-dependent "density" of superconducting electrons $n(z)$, momentum $q(z)$, and superconducting current density $j(z) \sim -|e|n(z)q(z)$ in an SN strip. For the $n(z)$ and direction of $B_{\rm in}$ shown, finite momentum $q_{\rm NCS}$ points against the $x$ axis.

a thin SN bilayer with thickness $d_S + d_N \ll \lambda$ ($\lambda \sim n^{-1/2}$ is the London penetration depth), one may neglect the magnetic field arising from the Meissner currents and choose $\mathbf{A} = (B_{\rm in}z, 0, 0)$ where $-(d_S + d_N)/2 < z < (d_S + d_N)/2$. In the case where $n(z) = \text{const}$ the total current $I \sim \int j(z)dz = 0$ when the *thickness-averaged momentum* $q_0 = \int qdz/(d_S + d_N) = \nabla\phi = 0$. However, in the case where $\nabla n(z) \neq 0$, one needs finite $q_0 = q_{\rm NCS}$ to have $I = 0$. This describes the *orbital* mechanism of finite momentum superconductivity in the SN strip. From a mathematical point of view the presence of both thickness-averaged $\nabla n$ and $B_{\rm in}$ breaks the symmetry in the SN strip, and the vector $\nabla n \times B_{\rm in}$ defines the particular direction and value of $q_{\rm NCS}$.

From the above consideration it is clear that a finite momentum state of this type has to exist in any superconductor having finite $\nabla n$ and $B_{\rm in}$. Here we prove this for an SN bilayer where the S layer is a dirty superconductor with large resistivity (small diffusion coefficient $D_S$) in the normal state and the N layer is a low-resistivity normal metal having large diffusion coefficient $D_N \gg D_S$. In this system, due to the noticeable contribution of proximity-induced superconductivity in the N layer to total $L_k$, we expect to have a large difference between $L_k(I)$ and $L_k(-I)$ which is easy to observe experimentally and which is a fingerprint of FMS. This system also has the diode

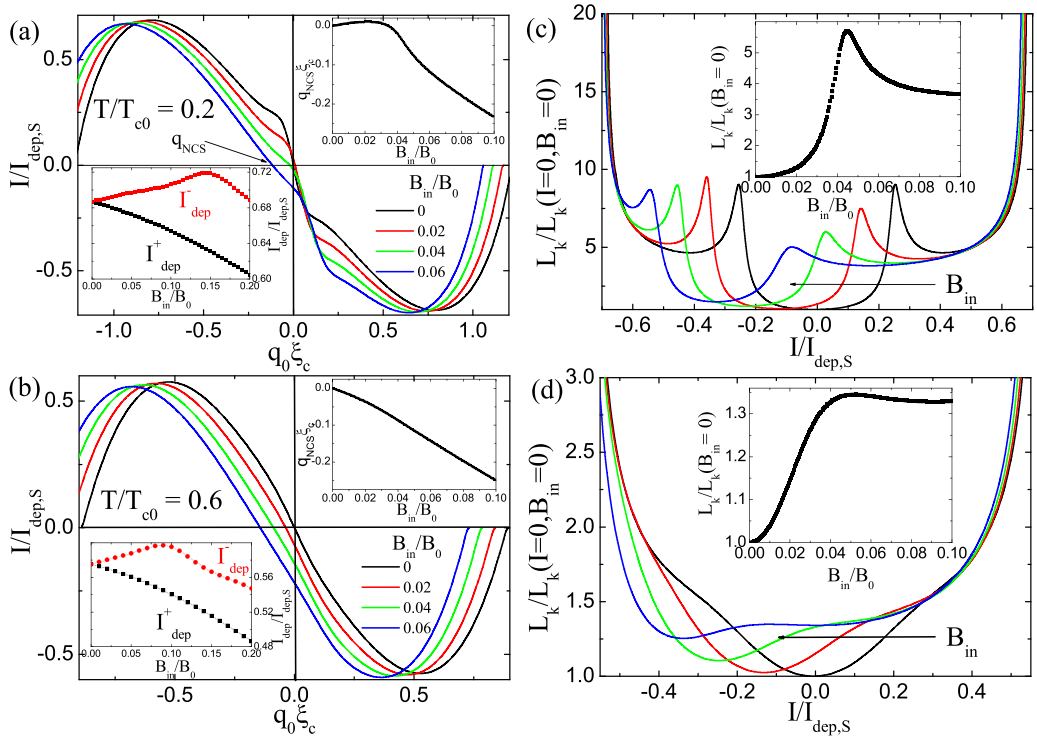


FIG. 3. Theoretical dependencies of current on momentum [(a) and (b)] and kinetic inductance on current [(c) and (d)] in an SN bilayer at different in-plane magnetic fields and two temperatures $T = 0.2$ and $0.6T_{c0}$. In the insets of (a) and (b) we present the field dependencies of $I^{\pm}_{\rm dep}$ and finite momentum $q_{\rm NCS}$ at $I = 0$. In the insets (c) and (d) we show the calculated field dependence of $L_k$ in the zero-current state. Here, $B_0 = \Phi_0/2\pi\xi_c^2$, and $I_{{\rm dep},S}$ is the depairing current of a single S layer with thickness $d_S$.

effect, as was found earlier in Ref. [18], but its relation with FMS was not discussed there. Another motivation to study this system comes from recent experiments where the diode effect was observed in somewhat similar superconducting hybrids in the presence of an in-plane magnetic field [17,19–22], where we also expect a contribution of the orbital mechanism to the SDE.

The structure of this paper is as follows. In Sec. II we present our theoretical results with characteristics of FMS which has an orbital mechanism in an SN bilayer. In Sec. III A we describe the experimental methods used to study FMS in the SN bilayer. In Secs. III B and III C we present experimental results which demonstrate that we have a finite momentum state in our superconducting hybrid and some unexpected properties of this state. In Sec. IV we discuss our findings that the orbital mechanism of FMS has a distinctive thickness dependence (the thickness dependence can be used to distinguish the orbital mechanism from the mechanism connected with spin-orbit coupling) and that our SN hybrid has the expected behavior. In the same section we discuss other experiments on FMS and the diode effect and their relation with our results. In Sec. V we present our conclusions.

## II. THEORETICAL RESULTS

We start with a presentation of our theoretical results. In Fig. 3 we show the calculated $I(q_0, B_{\rm in})$ and $L_k(I, B_{\rm in})$ for an SN strip having the following parameters: $d_S = d_N = 4\xi_c$ [$\xi_c = (\hbar D_S/k_B T_{c0})^{1/2}$, where $T_{c0}$ is the critical temperature of the S layer] and the ratio $D_N/D_S = 100$. To find $I(q_0, B_{\rm in})$ and $L_k(I, B_{\rm in})$, we use the Usadel model (details of the calculations are presented in Appendix A). We choose two temperatures, $T = 0.2$ and $T = 0.6T_{c0}$, which correspond to different physical situations. At $T = 0.2T_{c0}$ the contribution of the N layer is dominant in $L_k$ at small fields and currents, while at $T = 0.6T_{c0}$ the N layer has a much smaller contribution to the transport properties. In both cases, finite field-controlled $q_{\rm NCS}$ appears [see upper insets in Figs. 3(a) and 3(b)] leading to asymmetry of $I(q_0)$ and nonreciprocal $L_k(I)$. At $T = 0.2T_{c0}$ and small $B_{\rm in}$, $q_{\rm NCS} > 0$ because $n$ is larger in the N layer (in Fig. 2 the opposite situation is shown, which is true for our SN strip at $T = 0.6T_{c0}$ at any $I$ and $B_{\rm in}$). At large $B_{\rm in}$ and currents close to $I^{\pm}_{\rm dep}$, superconductivity in the N layer becomes suppressed, and $L_k$ increases. The transition between the states with different $L_k$ is accompanied by the appearance of a peak in the dependencies $L_k(I)$ and $L_k(B_{\rm in})$; see Figs. 3(c) and 3(d). Note that this peak is absent in ordinary superconductors [see Fig. 1(d)] and/or much less pronounced in SN bilayers with the small contribution of the N layer to the transport properties [see Fig. 3(d)].

In the finite momentum state there is a difference between positive and negative depairing currents [see bottom insets in Figs. 3(a) and 3(b)]. $I^{-}_{\rm dep}$ is larger than $I^{+}_{\rm dep}$ because the current-induced momentum partially compensates the field-induced momentum in the N layer leading to the recovery of proximity-induced superconductivity. At small $B_{\rm in}$ it provides even an increase in $I^{-}_{\rm dep}$: A physically similar increase in $I_c$ is

realized in a superconducting strip with nonequivalent edges that is in an out-of-plane magnetic field [23].

## III. EXPERIMENT

### A. Methods

The experiment was performed with MoN/Cu strips. MoN is a dirty superconductor with resistivity in the normal state $\rho = 150\,\mu\Omega\,\mathrm{cm}$, while Cu is a low-resistivity metal (40-nm-thick Cu has $\rho = 2.4\,\mu\Omega\,\mathrm{cm}$ at $T = 10$ K). The MoN/Cu bilayers are grown by magnetron sputtering with a base vacuum level of the order of $1.5\times10^{-7}$ mbar on standard silicon substrates without removing the oxide layer and at room temperature. First, Mo is deposited in an atmosphere consisting of the gas mixture Ar:$N_2$ = 10:1 at a pressure of $1\times10^{-3}$ mbar, and than Cu is deposited in an argon atmosphere at a pressure of $1\times10^{-3}$ mbar. Finally, MoN/Cu strips are made with the help of mask-free optical lithography.

The majority of measurements were performed for thick $d_{\mathrm{MoN}} = 40$ nm, $d_{\mathrm{Cu}} = 40$ nm samples. Altogether we have four long strips (samples A1–A4; width 4 μm, length 3 mm) and nine short bridges (samples B1–B9; width 4 μm, length 100 μm). All measured samples (samples A1, A2, A4, B2, and B3) have nearly the same sheet resistance $R_s(300\ \mathrm{K}) = 1\ \Omega$ and $R_s(T = 10\ \mathrm{K}) = 0.6\ \Omega$ (variation from sample to sample is less than 10%) and critical temperature $T_c = 7.87$ K defined from the condition that resistance $R(T_c) = 0.5R(10\ \mathrm{K})$.

In addition, we made and studied two-times-thinner [MoN(20 nm)/Cu(20 nm)] reference long strips with the same width and length as the thicker MoN/Cu strips to check the thickness dependence of the finite momentum state and verify its orbital nature. Their characteristics are presented in Appendix C.

The current-voltage ($I$-$V$) characteristics were measured using the four-probe method. Examples of the $I$-$V$ curves are shown in Fig. 4 for sample A2 (in the inset we present the temperature dependence of $I_c$ at $B_{\mathrm{in}} = 0$). From these measurements we extracted critical currents $I_c^{\pm}$ (see arrows in Fig. 4) as a function of $B_{\mathrm{in}}$.

The impedance $Z = Z_{\mathrm{re}} + iZ_{\mathrm{im}}$ of the MoN/Cu strips was measured using a Stanford Research SR830 lock-in amplifier. For measurements the four-probe method was used. An excitation signal with frequency $\nu = 100$ kHz and voltage 50 mV from the SR830's internal generator was supplied through a 1-kΩ resistor. Signal from the sample was applied to the differential input of the SR830 through the central electrodes of two coaxial cables. These measurements allowed us to find the field and current dependence of inductance $L = Z_{\mathrm{im}}/2\pi\nu$. The same device was used to measure the first ($R_\omega$) and second ($R_{2\omega}$) harmonic signals of the ac resistance at a frequency of 130 Hz.

In our strips we have a noticeable contribution of the geometric inductance $L_g$ to the total inductance. Using the expression below for a strip with length $l$, width $w$, and thickness $d$ in the limit $l \gg (w + d)$ [24]

$$L_g = \frac{\mu_0 l}{2\pi}\left[\ln\left(\frac{2l}{w+d}\right) + 1/2\right], \tag{1}$$

we find, for our long strips, $L_g \simeq 4.7$ nH.

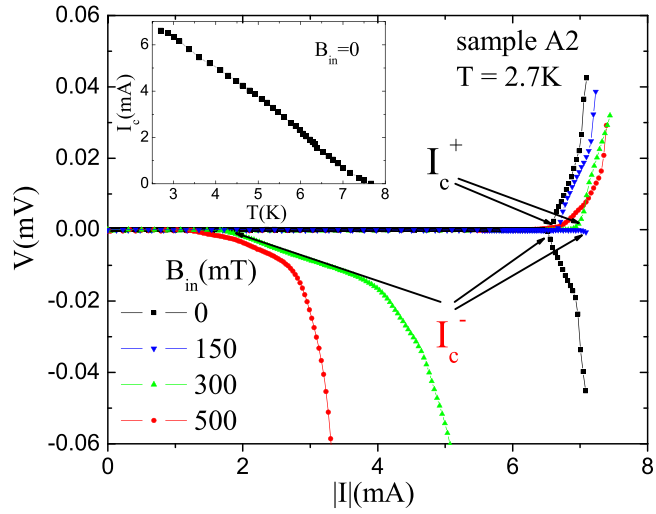


FIG. 4. Current-voltage characteristics of sample A2 at different $B_{\mathrm{in}}$ and $T = 2.7$ K (negative voltage corresponds to negative current, while in the $x$ axis we show the absolute value of the current); arrows indicate $I_c^{\pm}$. In the last points of the $I$-$V$ curves there is a jump to the normal state (not shown here). The $I$-$V$ curves are not hysteretic before the transition to the normal state. Critical currents (their absolute values) are determined from condition $|V|(I = I_c^{\pm}) = 0.5\,\mu$V. After the transition to the normal state the sample returns to the superconducting state at $I_r \simeq 1.6$ mA (when $I_c^{\pm} > I_r$), which practically does not depend on the magnetic field and current direction. In the inset we show the temperature dependence $I_c(T)$ at $B_{\mathrm{in}} = 0$.

### B. Results below $T_c$

In Fig. 5 (see also Fig. 8 in Appendix B) we present $L_k(I)$ at different $B_{\mathrm{in}}$ and $I_c{\pm}(B_{\mathrm{in}})$ at two temperatures, 4.6 and 2.7 K, which roughly correspond to the two temperatures presented in Fig. 3. The main result is that in an in-plane field, the inductance $L$ is nonreciprocal, and this is the *main* proof that the MoN/Cu strip has finite momentum at $I = 0$. Although we know $L(I, B_{\mathrm{in}})$, this does not allow us to find $q_{\mathrm{NCS}}$ and its dependence on the magnetic field: For that, one has to know, additionally, $I(q_0)$ at least at one value of $q_0$.

The experimental dependence $L(B_{\mathrm{in}})$ at zero current and evolution of $L(I)$ with increasing $B_{\mathrm{in}}$ follow the theoretical prediction at all magnetic fields with the important difference, for the following discussion of the diode effect, that in the experiment we do not reach the depairing current $I_{\mathrm{dep}}^{\pm}$ where the theoretical $L_k$ diverges [compare Figs. 5(a) and 5(b) with Figs. 3(c) and 3(d)]. This occurs probably due to the presence of edge defects which allow entry of *out-of-plane* vortices at $I < I_{\mathrm{dep}}^{\pm}$, and the entry of these vortices does not allow us to approach the depairing current. Indeed, an image of a similar Cu/MoN strip made with the help of an electron microscope (see, for example, Fig. 1 in Ref. [25]) shows that we have edge roughnesses with a size of about 100 nm. The idea of vortex entry at $I > I_c^{\pm}$ is supported by the experimental $I$-$V$ curves (see Fig. 4): Above the critical current the SN strip transits to a low-resistivity state which resembles a flux flow regime.

In contrast to the inductance, our experimental results on the superconducting diode effect are controversial. We find a sample-dependent difference between $I_c^{+}$ and $I_c^{-}$ [in contrast

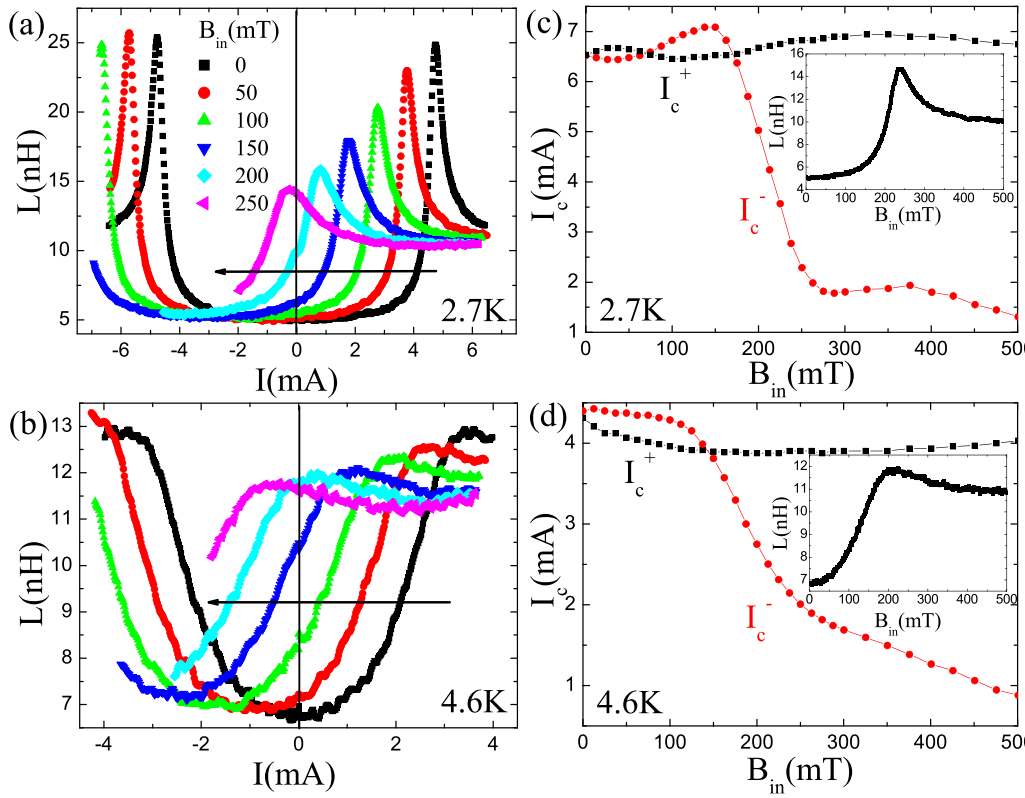


FIG. 5. (a) and (b) Evolution of the current-dependent inductance of a MoN/Cu strip (sample A2) in the superconducting state with increasing in-plane magnetic field at $T = 2.7$ K and $T = 4.6$ K, respectively. In (c) and (d) we present the field-dependent critical current and field-dependent inductance at $I = 0$.

to the almost not sample-dependent $L(I, B_{\rm in})$], and besides, the SDE has unexpected values and sign at relatively large $B_{\rm in}$ for all studied samples (compare Figs. 3, 5, 8, and 9). At magnetic field $B_{\rm in} \lesssim 150$ mT the sign and value of the SDE mainly coincide with prediction of our theory for samples A1, A4, and B4, while for samples A2 and B3 there is a sign change of the diode effect with increasing $B_{\rm in}$. At $B_{\rm in} \gtrsim 150$ mT we have $I_c^- \ll I_c^+$ for all samples. The large difference [ratio $\eta = 2|I_c^- - I_c^+|/(I_c^- + I_c^+) > 1$] and its "wrong" sign cannot be explained by our theory, which predicts $I_c^- = I_{\rm dep}^- \gtrsim I_c^+ = I_{\rm dep}^+$.

It could be supposed that in our experiment, together with the in-plane field, there is a small out-of-plane field $B_{\rm out}$ (due to imperfect alignment of the sample holder along the superconducting coil which is a source of our magnetic field). Even small $B_{\rm out}$, in comparison to $B_{\rm in}$, strongly suppresses $I_c$ and in the presence of edge defects may lead to the SDE, which also has an orbital nature because it originates from the combined effect of Meissner and transport currents [23]. This type of SDE was found experimentally in different superconductors [25–30]. Note that probably the same mechanism is responsible for the SDE observed in a $NbSe_2$ bridge [31], which follows from its sample-dependent character and the nearly linear decay of $I_c$ at small fields $\lesssim \Phi_0/2\pi\xi w$, which is evident in the edge-barrier-controlled $I_c^{\pm}$ [32]. In a strip or bridge with an edge defect the strength of this type of SDE is controlled by the parameters of the defect, and $\eta$ may be larger than unity as follows from Ref. [25], which resembles our result at large $B_{\rm in}$.

Therefore we measured $L(I, B_{\rm out})$ and $I_c^{\pm}(B_{\rm out})$; see Fig. 6. The influence of bulk pinning in our hybrid is negligible, at least in the field range used, as follows from the typical edge-barrier-controlled field-dependent $I_c^{\pm}(B_{\rm out})$ [32] [$I_c^{\pm}$ drops nearly linearly at low fields, and $I_c^{\pm} \sim 1/B_{\rm out}$ at large fields; see Fig. 6(d)]. We find nearly reciprocal $L(I)$, while there is a small superconducting diode effect, comparable in value to the SDE at $B_{\rm in} \lesssim 150$ mT and which also may change sign [see Fig. 6(c)]. The sign change does not follow from the model of Ref. [23], and in principle it may appear if there are defects on opposite edges of the strip with different magnetic-field-controlled "strengths" leading to different degrees of suppression of the edge barrier. The edge defects give a nonreciprocal contribution to the total $L_k$ but on the scale of about the defect size (∼100 nm) along the strip, which is several orders of magnitude smaller than its length (3 mm). As a result it is difficult to observe nonreciprocal $L(I)$ in an out-of-plane field.

From comparison of Figs. 5 and 6 we conclude that even if there is finite $B_{\rm out}$ in the experiment with an in-plane field, it cannot explain the large difference between $I_c^+$ and $I_c^-$ at $B_{\rm in} \gtrsim 150$ mT because $B_{\rm out}$ suppresses them on an equal footing. Besides, at $B_{\rm out} = 5$ mT [$I_c^{\pm}(5\ {\rm mT}) \sim I_c^{\pm}(0)/2$] the kinetic inductance practically does not depend on the current, while in an in-plane field $L$ varies with the current even at $B_{\rm in} = 250$ mT [$I_c^-(250\ {\rm mT}) \sim I_c^{\pm}(0)/3$]. Therefore we exclude the influence of $B_{\rm out}$.

Sample-dependent $I_c^{\pm} < I_{\rm dep}^{\pm}$ allows us to suppose that out-of-plane vortices enter the SN strip via local sample-

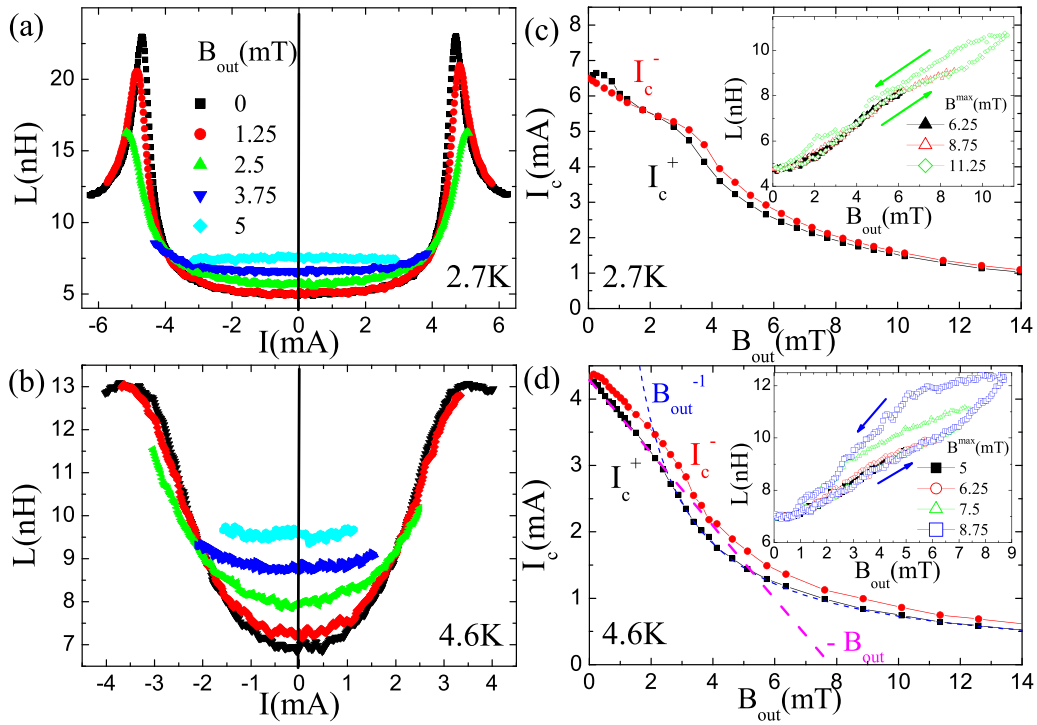


FIG. 6. (a) and (b) Evolution of the current-dependent inductance of a MoN/Cu strip (sample A2) with increasing out-of-plane magnetic field at $T = 2.7$ K and $T = 4.6$ K, respectively. In (c) and (d) we present the field-dependent critical currents and inductance. The dependence $L(B_{\text{out}})$ for sweeping up and down field is hysteretic for relatively large amplitudes of $B_{\text{out}}$, which we relate with trapped out-of-plane vortices due to the edge barrier for vortex entry and exit.

dependent edge defects at $I > I_c^{\pm}$ and this launches the resistive state: On the experimental $I$-$V$ curves there are vortex flow branches above $I_c^{\pm}$. At small fields, when the proximity-induced superconductivity in the Cu layer is slightly suppressed by $B_{\text{in}}$, there is proportionality: $I_c \sim I_{\text{dep}}$ (coefficient proportionality is sample dependent). Because a defect may have variation in its properties across the thickness of the MoN/Cu strip, this may lead to change in the sign of the diode effect, similar to the change in sign observed in an out-of-plane field. Obviously, our one-dimensional (1D) model cannot catch this effect.

A large in-plane field more strongly suppresses proximity-induced superconductivity in the Cu layer. Positive current suppresses it even more, and we effectively have a single S layer with weak field dependence of $I_c^+$ at $B_{\text{in}} \lesssim \Phi_0/d_S^2 \sim$ 1300 mT (at this or larger field we expect the entry of in-plane vortices in the S layer according to Ref. [33]), which we observe in the experiment. Negative current partially recovers superconductivity in the N layer [it is seen from the decrease in experimental $L(I)$ at large $B_{\text{in}}$], and this may lead to the appearance of in-plane vortices in the N layer near the SN interface at field $B_{\text{in}} \sim \Phi_0/(d_S + d_N)^2 \sim 320$ mT, which is near our experimental value. In-plane vortices should favor the entry of out-of-plane vortices, and this may suppress the critical current and change the relation between $I_c$ and $I_{\text{dep}}$. This is a possible but speculative scenario. Theoretical description of out-of-plane vortex entry into an SN strip with thickness-dependent "density" $n$, finite momentum $q_0$, and the possible existence of a row of in-plane vortices located on or close to the SN interface is a rather complicated 3D problem which needs separate study.

Single and multiple sign changes of the diode effect with increasing in-plane or out-of-plane magnetic field were observed earlier in Refs. [21,22,34,35] and predicted theoretically in Refs. [15,36] for a noncentrosymmetric superconductor. From those theoretical predictions it follows that together with sign change of the SDE there is a strong change in $I(q)$ (see Fig. 5 in Ref. [15] and Fig. 2 in Ref. [36]) and, hence, $L_k(I)$. In our system we do not observe drastic variation of $L_k(I)$ when sign change of the diode effect occurs and $L_k(I)$ evolves with increasing $B_{\text{in}}$ as our theory predicts. In Refs. [21,22,34,35], $L_k(I)$ was not measured, and it is difficult to interpret the origin of the effect.

### C. The diode effect and nonreciprocal resistivity near $T_c$

When approaching the critical temperature, $I_c^{\pm}$ decreases; however, still there is a diode effect, and $V(I) \neq -V(-I)$: See Fig. 7. It is known that thermal fluctuations allow vortices (we keep in mind out-of-plane vortices) to enter the superconducting strip at currents less than $I_c$. The probability for a vortex to overcome the edge barrier is proportional to the Arrhenius factor $\exp(-dF(I)/k_BT)$, where $dF(I)$ is the current-dependent height of the edge barrier, which goes to zero at $I = I_c$ and is proportional to the vortex energy at zero current: $dF \sim F_0 = \Phi_0^2 d/16\pi^2\lambda^2$ [37–39]. At $T \sim T_c$, both $I_c$ and $F_0$ vanish, which increases the impact of fluctuations. As a result, near $T_c$ the resistance $R$ is finite even at $I \to 0$, and it

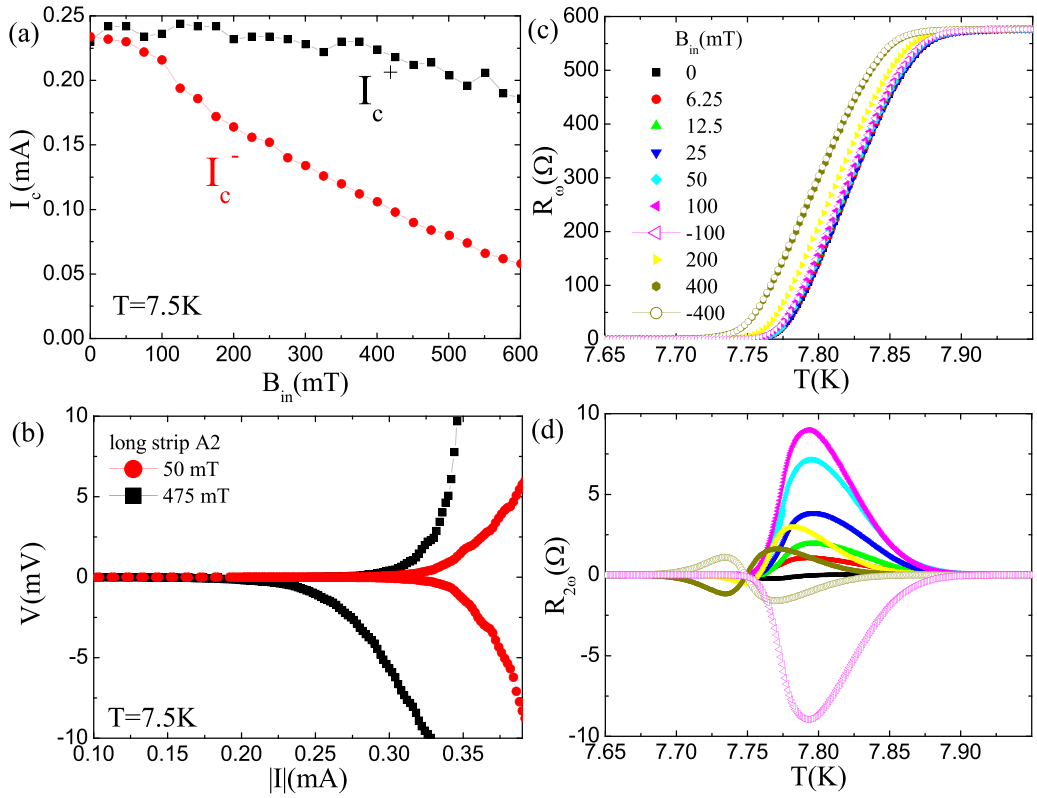


FIG. 7. (a) Field-dependent critical currents $I_c^{\pm}$ of sample A2 at $T = 7.5$ K. (b) Current-voltage characteristics of sample A2 at different $B_{\rm in}$. (c) and (d) Temperature dependence of the first and second harmonics of $I$-$V$ characteristics at different in-plane magnetic fields.

could be nonreciprocal in the case of different $I_c^{\pm}$ because of $dF(I^+) \neq dF(I^-)$.

An additional mechanism which may contribute to nonreciprocal $R$ is the current-dependent viscosity of vortex motion. Indeed, a transport current with one direction suppresses proximity-induced superconductivity in the N layer more strongly than the current with the opposite direction, which should affect the vortex velocity $v$ and voltage $V \sim v$. Our measurements of the first and second harmonics of $I$-$V$ characteristics confirm the existence of nonreciprocal resistance at finite $B_{\rm in}$ near $T_c$ [see Figs. 7(c) and 7(d)].

In earlier studies, finite $R_{2\omega}$ near $T_c$ was found for various hybrid superconducting structures placed in an in-plane magnetic field, and its origin was related with spin-orbit coupling [19,40–42]. Our experiment demonstrates a qualitatively similar result in the MoN/Cu hybrid, where we have an orbital mechanism of the finite momentum state, resulting in the diode effect and nonreciprocal resistance near the critical temperature. We believe that the same orbital mechanism has to exist in Refs. [19,40–42] and compete with spin-orbit interaction.

## IV. DISCUSSION

The proposed orbital mechanism of the finite momentum state in hybrid superconductors is the finite size (thickness) effect. We theoretically find that at relatively large $B_{\rm in}$, $q_{\rm NCS} \sim -B_{\rm in}(d_S + d_N)2\pi/\Phi_0$ for different thicknesses of S and N layers [for the parameters of the SN bilayer from Fig. 3, $q_{\rm NCS} \simeq -B_{\rm in}(d_S + d_N)2\pi/3\Phi_0$]. This means that when the thickness of the SN bilayer goes to zero, $q_{\rm NCS} \to 0$ and the orbital mechanism disappears (the same is valid when $d_N \to 0$). This gives us a way to check the origin of FMS in the experiment: One may study the thickness dependence of $L_k(I, B_{\rm in})$ because for smaller thickness a larger $B_{\rm in}$ is needed to have the same $q_{\rm NCS}$. Indeed, we find that for a two-times-thinner sample, MoN(20 nm)/Cu(20 nm), the change in $L(I)$ is less sensitive to $B_{\rm in}$ [compare Fig. 10(a) with Figs. 5(a) and 5(b)] than for a thick strip, which qualitatively coincides with our calculations [compare Figs. 3(b) and 3(d) with Figs. 10(c) and 10(d)].

Our experimental results indicate that one should be careful with interpretation of experiments on the diode effect. We observe sign change of the diode effect with increasing magnetic field in two (one long and one short) thick samples and the absence of sign change of the diode effect in another two (one long and one short) thick samples at $B_{\rm in} \lesssim 150$ mT while $L(I, B_{\rm in})$ and, hence, $I(q)$ were almost the same for all long samples. This means that an additional factor, one that is not intrinsic to the character of a given material, may play a role. In our case we believe that sample-dependent edge defects are responsible for the observed effect. In this respect, measurements of $L_k(I, B_{\rm in})$ give more reliable information about the intrinsic origin of the finite momentum state than measurements of $I_c^{\pm}(B_{\rm in})$. Indeed, if there is strong variation in the superconducting properties along the sample, but over a small distance, this variation weakly affects the total kinetic inductance, but it may strongly affect the critical current because the critical current is determined by the "weakest" place.

At $B_{\rm in} \gtrsim 150$ mT for all thick samples we find sign change of the diode effect and its considerably larger value in comparison with theoretical expectations. At the same time we do not observe any qualitative changes in $L(I)$. We believe that this could be connected with the appearance of in-plane vortices in the SN bilayer. If this is true, it is also a finite thickness effect, and with decreasing thickness of the SN bilayer, in-plane vortices (and sign change of the diode effect) should appear at larger field. A somewhat similar effect appears in the thin strips, where we do not have sign change of the diode effect at 2.7 K for any of the three samples studied up to $B_{\rm in} = 500$ mT and at 4.6 K the sign change exists only for one sample.

In Ref. [19] the diode effect was observed in a multilayered Nb/V/Ta strip with thickness $d = 120$ nm and width $w = 50\,\mu$m. At low temperature, the SDE vanished, which is in contrast to the results of Refs. [17,20–22] and our work, where the diode effect becomes more pronounced at low $T$. The width of the Nb/V/Ta strip greatly exceeds the effective Pearl magnetic field penetration depth $\lambda^2/d$ except at $T \sim T_c$ [we assume that $\lambda(0) = 120$ nm as in dirty Nb because the zero-temperature coherence length $\xi(0) = 13$ nm of the multilayered strip is close to the $\xi$ of dirty Nb]. This means that the current distribution is nonuniform over the width of the Nb/V/Ta strip, which automatically means that the critical current has to be much smaller than the depairing current and the resistive state is connected with entry and motion of out-of-plane vortices. The nonuniform current distribution may lead to vortex pinning at low temperature, which destroys the experimentally observed diode effect.

In Al/InGaAs/InAs/InGaAs heterostructures the SDE was found and explained by the interplay between diamagnetic and external currents [22], which qualitatively coincides with the mechanism of the diode effect in an SN bilayer proposed in Ref. [18], in this paper, and in Ref. [23] for a superconducting strip with nonequivalent edges that is in an out-of-plane magnetic field. The assumption of the authors of Ref. [22] that different layers in the heterostructure have different currents may be reformulated in terms of the different densities of the superconducting electrons and finite $\nabla n$, which has to lead to finite $q_{\rm NCS}$ when there is an in-plane magnetic field. In terms of Ref. [22] we have a strong-coupling regime between the S and N layers, and in our case if in-plane vortices appear at large $B_{\rm in}$, they should be more like Abrikosov vortices than Josephson ones.

In Refs. [17,20,21] the SDE was observed in superconductor/normal metal/superconductor (SNS) Josephson junctions (JJs), and hence our results cannot be applied directly to those systems. However, all studied junctions have hybrid SN banks where an in-plane magnetic field should produce FMS. This raises the question, Could finite $q_{\rm NCS}$ in the SN banks affect the transport properties of JJs even if in the N weak link there is no $\nabla n$ or it is small? To answer this question, one has to calculate the transport properties of an SN/N/SN junction taking into account the finite thicknesses of SN banks and the normal-metal weak link, which is a difficult 2D problem. Therefore at the moment we cannot claim that the orbital mechanism is involved in the diode effect observed in Refs. [17,20,21], although the results from those works look qualitatively similar to our results.

## V. CONCLUSION

We demonstrate the appearance of a finite momentum state in an SN bilayer placed in an in-plane magnetic field. Experimentally, the presence of FMS is proven via observation of nonreciprocal inductance $L(I) \neq L(-I)$ in several MoN/Cu strips that are in an in-plane magnetic field. The FMS has an orbital nature as follows from the experiment with samples having different thicknesses and the expected zero or negligible contribution of spin-orbit coupling in our system.

We also experimentally observe the superconducting diode effect, but in contrast to results with $L(I, B_{\rm in})$ it has rather cumbersome sample-dependent behavior. We speculate that this could be connected with the presence of sample-dependent edge defects and the appearance of in-plane vortices in large enough $B_{\rm in}$.

Taking into account our results and the discussion in the Introduction, we may claim that the finite momentum state is not an elusive or rare phenomenon in superconducting structures. Any nonuniformities (material or geometric) lead to $\nabla n \neq 0$, and in the presence of a magnetic field the particular direction appears along which there is a difference in critical currents (the SDE) and nonreciprocal $L_k$. If the diode effect originates from local edge defects (as in the case of a superconducting strip placed in an out-of-plane field), it may not lead to noticeable nonreciprocal $L_k$ of a whole sample due to the local nature of FMS in this case.

## ACKNOWLEDGMENT

This work is supported by the Russian Science Foundation (Project No. 23-22-00203).

## APPENDIX A: MODEL

To calculate the transport properties (critical current, kinetic inductance) of the SN bilayer, we use the one-dimensional Usadel equation for normal $g$ and anomalous $f$ quasiclassical Green's functions [43]. With standard angle parametrization $g = \cos\Theta$ and $f = \sin\Theta \exp(i\varphi)$ the Usadel equations in different layers can be written as

$$\hbar D_S \frac{\partial^2 \Theta_S}{\partial z^2} - (\hbar\omega_k + D_S \hbar q^2 \cos\Theta_S)\sin\Theta_S + 2\Delta\cos\Theta_S = 0, \tag{A1}$$

$$\hbar D_N \frac{\partial^2 \Theta_N}{\partial z^2} - (\hbar\omega_k + D_N \hbar q^2 \cos\Theta_N)\sin\Theta_N = 0, \tag{A2}$$

where subscripts $S$ and $N$ refer to superconducting and normal layers, respectively. Here, $D$ is the diffusion coefficient for the corresponding layer, $\hbar\omega_k = \pi k_B T(2k+1)$ are the Matsubara frequencies ($k$ is an integer number), $\hbar q = \hbar(\nabla\varphi + 2\pi\,\mathbf{A}/\Phi_0) = \hbar(q_0 + 2\pi\,\mathbf{A}/\Phi_0)$ is the momentum of Cooper pairs, $\varphi$ is the phase of the order parameter, $\mathbf{A}$ is the vector potential, and $\Phi_0 = \pi\hbar c/|e|$ is the magnetic flux quantum. $\Delta$ is the superconducting order parameter, which satisfies the self-consistency equation

$$\Delta \ln\left(\frac{T}{T_{c0}}\right) = 2\pi k_B T \sum_{\omega_k > 0}\left(\sin\Theta_S - \frac{\Delta}{\hbar\omega_k}\right), \tag{A3}$$

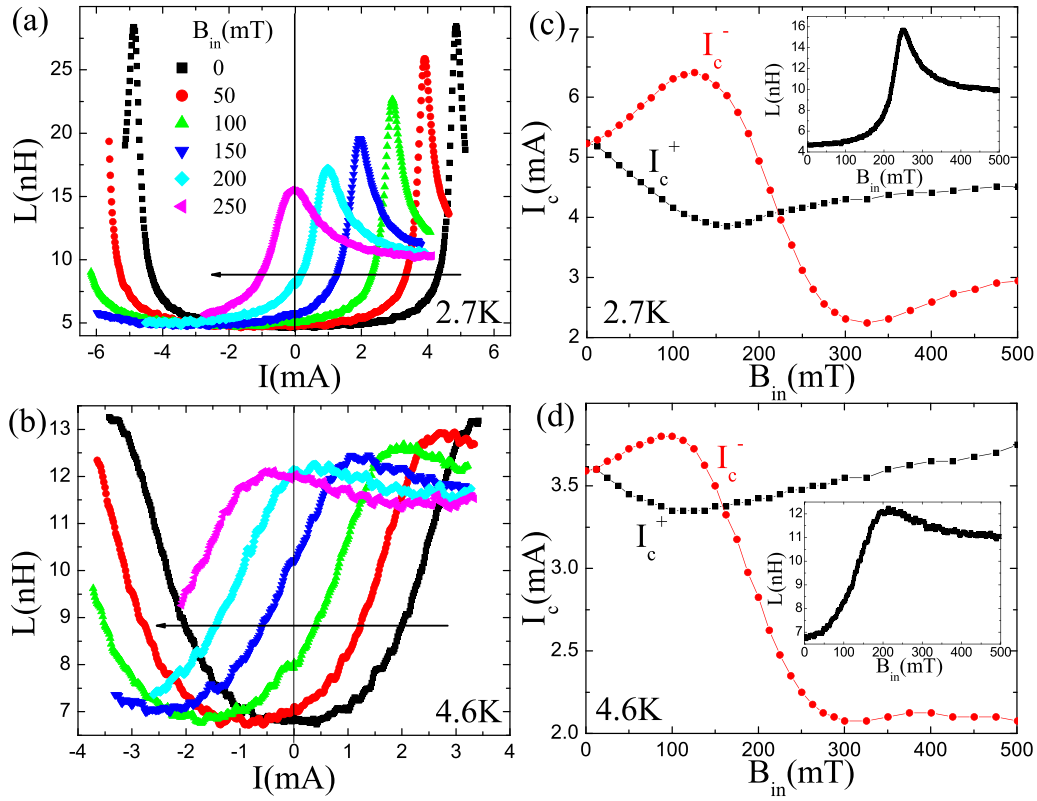


FIG. 8. (a) and (b) Evolution of the current-dependent inductance of a MoN/Cu strip (sample A4) with increasing in-plane magnetic field at $T = 2.7$ K and $T = 4.6$ K, respectively. In (c) and (d) we present the field-dependent critical current and inductance.

where $T_{c0}$ is the critical temperature of a single S layer in the absence of a magnetic field. These equations are supplemented by the Kuprianov-Lukichev boundary conditions on the SN interface [44]:

$$D_S \frac{d\Theta_S}{dz} = D_N \frac{d\Theta_N}{dz}. \tag{A4}$$

For simplicity we consider the case with zero barrier between layers and continuous $\Theta$ on the SN interface. For interfaces with a vacuum we use the boundary condition $d\Theta/dz = 0$.

We assume that the thickness $d_S + d_N$ of the SN strip is much smaller than the London penetration depth $\lambda$ while the width $w$ is smaller than the Pearl penetration depth $\Lambda = \lambda^2/(d_S + d_N)$, which allows us to neglect the effect of superconducting screening on the vector potential and magnetic field. We choose vector potential $\mathbf{A} = (-B_{\rm in} z, 0, 0)$ with thickness-averaged $\int \mathbf{A} dz = 0$ [here, $-(d_S + d_N)/2 < z < (d_S + d_N)/2$].

To calculate the current density $j$, the "density" of superconducting electrons $n$, and the current $I = w \int j dz$, we use the standard expressions

$$j(z) = -\frac{2\pi k_B T}{|e|\rho} q(z) \sum_{\omega_k > 0} \sin^2\Theta = -|e| n(z) q(z) \frac{\hbar}{m}, \tag{A5}$$

$$n(z) = \frac{m}{\hbar} \frac{2\pi k_B T}{e^2 \rho} \sum_{\omega_k > 0} \sin^2\Theta = \frac{mc^2}{8\pi |e| \lambda^2(z)}, \tag{A6}$$

where $\rho = 2|e| D_{S,N} N(0)$ is the residual resistivity of the corresponding layer, $N(0)$ is the density of states of electrons per one spin at the Fermi level in the normal state [we assume identical $N(0)$ in the S and N layers], and $m$ is a "mass" of superconducting electrons.

Equations (A1)–(A3) are solved numerically by using an iteration procedure. For initial distribution $\Delta(z) = \text{const}$ and chosen $q_0$ and $B_{\rm in}$, we solve Eqs. (A1) and (A2) (in the numerical procedure we use the Newton method combined with the tridiagonal matrix algorithm). The found solution $\Theta(z)$ is inserted into Eq. (A3) to find $\Delta(z)$, and then the iterations repeat until the relative change in $\Delta(z)$ between two iterations does not exceed $10^{-8}$. Length is normalized in units of $\xi_c = \sqrt{\hbar D_S / k_B T_{c0}}$, energy is in units of $k_B T_{c0}$, current is in units of depairing current $I_{{\rm dep},S}$ of a single S layer with thickness $d_S$, and the magnetic field is in units of $B_0 = \Phi_0/2\pi\xi_c^2$ [$B_0$ is smaller by a factor of 1.76 than the out-of plane second critical field $B_{c2}(T = 0)$ of a single S layer]. The typical step grid in the S and N layers is $\delta z = 0.1\xi_c$. In calculations we used the following parameters: $d_S = d_N = 4\xi_c$, $D_N/D_S = 100$ for a thick strip and $d_S = d_N = 2\xi_c$, $D_N/D_S = 80$ for a thin strip, which are not far from experimental values.

With calculated $I(q_0)$ we find the kinetic inductance per unit of length of the strip

$$L_k = -\hbar c^2 (dI/dq_0)^{-1}/2|e| \tag{A7}$$

and $I^{\pm}_{\rm dep}$ as the *absolute* value of the maximal positive and negative superconducting currents where $dI/dq_0 = 0$.

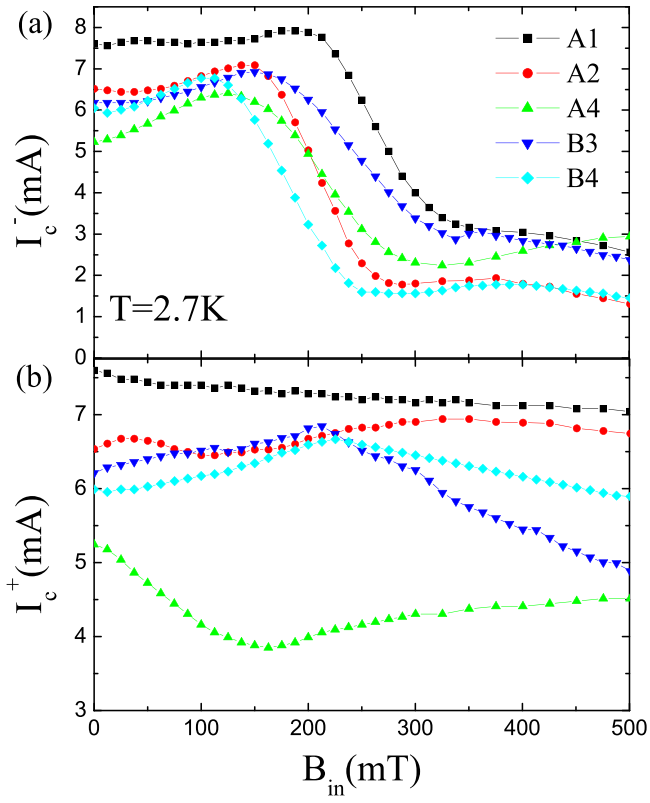


FIG. 9. (a) and (b) Field-dependent critical currents $I_c^{\pm}$ for different MoN/Cu strips (samples A1, A2, and A4, long strips; samples B3 and B4, short strips) at $T = 2.7$ K.

## APPENDIX B: RESULTS FOR DIFFERENT THICK SAMPLES

In Fig. 8 we show $L(I, B_{in})$ and $I_c^{\pm}(B_{in})$ for sample A4. While dependence $L(I, B_{in})$ is almost the same as for sample A2 (the same is valid for sample A1; results are not shown here), field dependencies of $I_c^{\pm}$ are quantitatively different at $B_{in} \lesssim 150$ mT and $T = 2.7$ K. We explain this by the presence of specific-to-each-sample edge defects.

In Fig. 9 we show sample-dependent $I_c^{\pm}(B_{in})$ for all of the studied strips (three long and two short) at $T = 2.7$ K. Despite quantitative differences, one may notice some general properties for all the strips. At weak fields ($B_{in} \lesssim 150$ mT), $I_c^-$ slightly increases, which is in accordance with our theory. However, then there is a sharp decrease in $I_c^-$, and it becomes much smaller than $I_c^+$, which is opposite to our model. In contrast, the critical current $I_c^+$ varies much more weakly while its field dependence changes from strip to strip.

## APPENDIX C: RESULTS FOR THINNER SAMPLES

In Figs. 10(a) and 10(b) we present results of transport measurements for two-times-thinner MoN/Cu long strips at $T = 4.6$ K (samples A1–A3; the width and length are the same as for thick long strips, $d_{MoN} = d_{Cu} = 20$ nm; $T_c = 7.37$ K; 20-nm-thick Cu has $\rho = 2.9$ μΩ cm at $T = 10$ K; the resistivity of the MoN layer is the same as for the 40-nm-thick layer). In Figs. 10(c) and 10(d) we show the-

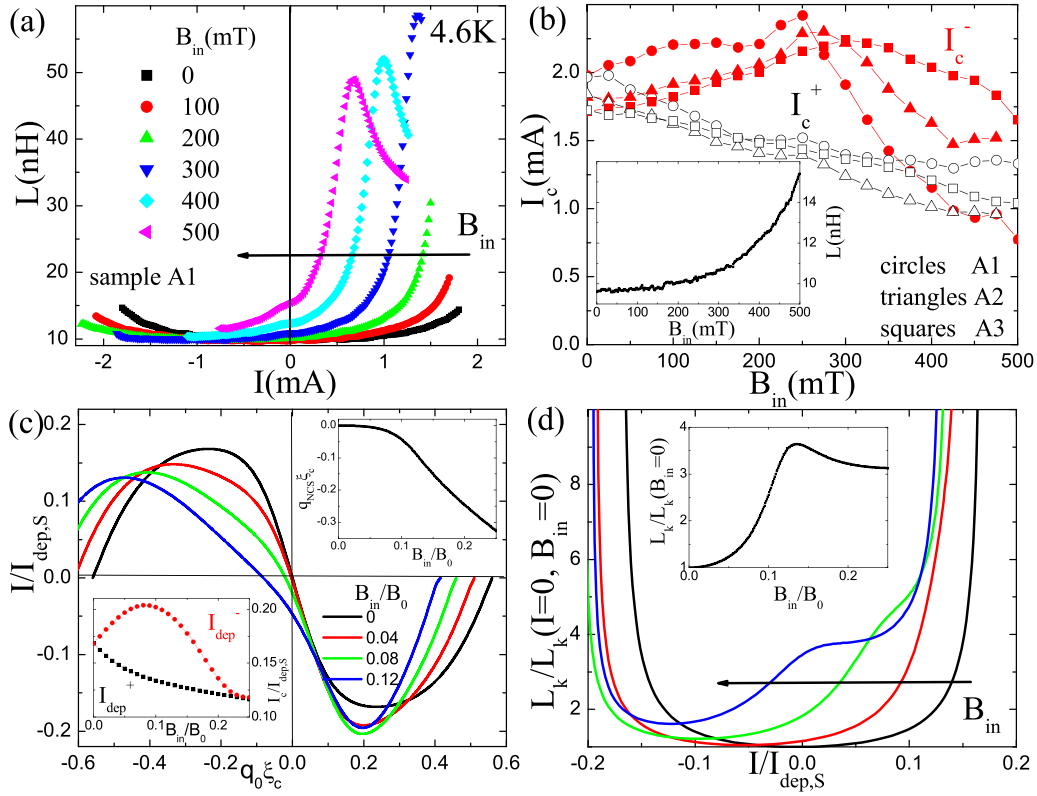


FIG. 10. (a) Evolution of the current-dependent inductance of a thin MoN(20 nm)/Cu(20 nm) strip (sample A1) with increasing in-plane magnetic field at $T = 4.6$ K. (b) Field-dependent positive and negative critical currents of samples A1–A3 at $T = 4.6$ K. In (c) and (d) we present the results of theoretical calculations for a thin SN strip.

oretical results ($d_S = d_N = 2\xi_c$, $D_N/D_S = 80$, $T = 0.6T_{c0}$). The inductance is nonreciprocal in the presence of an in-plane field, which is proof of the appearance of a finite momentum state, but we need a much larger field to have qualitatively the same change in $L$ as for a thick strip. From the experiment we conclude that our maximal accessible field ($B_{\text{in}} = 500\,\text{mT}$) does not destroy proximity-induced superconductivity in the Cu layer (at zero current) because we do not see a peak in dependence $L(B_{\text{in}})$ [see inset in Fig. 10(b)]. Qualitatively, the same results are obtained at $T = 2.7\,\text{K}$ (not shown here). These findings prove that we have in the experiment an orbital mechanism of the finite momentum state.

Sign change of the diode effect is observed only in sample A1 [see Fig. 10(b)] at 4.6 K, and for all studied samples it does not exist at 2.7 K [dependencies $I_c^{\pm}(B_{\text{in}})$ resemble ones for samples A2 and A3 at $T = 4.6\,\text{K}$ with a maximum of $I_c^{-}(B_{\text{in}})$ at ∼250 mT]. In this respect, results for thinner samples better follow our theoretical calculations with no sign change of the diode effect [see inset in Fig. 10(c)]. However, we cannot rule out its appearance at large fields, where $L$ should reach a peak in dependence $L(B_{\text{in}})$.


[1] P. Fulde and R. A. Ferrell, Superconductivity in a strong spin-exchange field, Phys. Rev. **135**, A550 (1964).

[2] S. Mironov, A. Mel'nikov, and A. Buzdin, Vanishing Meissner Effect as a Hallmark of in-Plane Fulde-Ferrell-Larkin-Ovchinnikov Instability in Superconductor-Ferromagnet Layered Systems, Phys. Rev. Lett. **109**, 237002 (2012).

[3] A. M. Bobkov and I. V. Bobkova, Enhancing of the critical temperature of an in-plane FFLO state in heterostructures by the orbital effect of the magnetic field, JETP Lett. **99**, 333 (2014).

[4] S. V. Mironov, D. Vodolazov, Y. Yerin, A. V. Samokhvalov, A. S. Melnikov, and A. Buzdin, Temperature Controlled Fulde-Ferrell-Larkin-Ovchinnikov Instability in Superconductor-Ferromagnet Hybrids, Phys. Rev. Lett. **121**, 077002 (2018).

[5] I. V. Bobkova and A. M. Bobkov, In-plane Fulde-Ferrel-Larkin-Ovchinnikov instability in a superconductor/normal metal bilayer system under nonequilibrium quasiparticle distribution, Phys. Rev. B **88**, 174502 (2013).

[6] J. A. Ouassou, W. Belzig, and J. Linder, Prediction of a Paramagnetic Meissner Effect in Voltage-Biased Superconductor–Normal-Metal Bilayers, Phys. Rev. Lett. **124**, 047001 (2020).

[7] M. Y. Levichev, I. Yu. Pashenkin, N. S. Gusev, and D. Yu. Vodolazov, Voltage controllable superconducting state in the multiterminal superconductor–normal-metal bridge, Phys. Rev. B **103**, 174507 (2021).

[8] V. D. Plastovets and D. Y. Vodolazov, Dynamics of domain walls in a Fulde-Ferrell superconductor, JETP Lett. **109**, 729 (2019).

[9] K. V. Samokhin and B. P. Truong, Current-carrying states in Fulde-Ferrell-Larkin-Ovchinnikov superconductors, Phys. Rev. B **96**, 214501 (2017).

[10] P. M. Marychev and D. Y. Vodolazov, Extraordinary kinetic inductance of superconductor/ferromagnet/normal metal thin strip in an Fulde-Ferrell state, J. Phys.: Condens. Matter **33**, 385301 (2021).

[11] V. M. Edelshtein, Characteristics of the Cooper pairing in two-dimensional noncentrosymmetric electron systems, Sov. Phys. JETP **68**, 1244 (1989).

[12] D. F. Agterberg, Novel magnetic field effects in unconventional superconductors, Phys. C (Amsterdam) **387**, 13 (2003).

[13] *Non-Centrosymmetric Superconductors*, edited by E. Bauer and M. Sigrist (Springer, Berlin, 2012).

[14] N. F. Q. Yuan and L. Fu, Supercurrent diode effect and finite-momentum superconductors, Proc. Natl. Acad. Sci. USA **119**, e2119548119 (2022).

[15] A. Daido, Y. Ikeda, and Y. Yanase, Intrinsic Superconducting Diode Effect, Phys. Rev. Lett. **128**, 037001 (2022).

[16] J. J. He, Y. Tanaka, and N. Nagaosa, A phenomenological theory of superconductor diodes, New J. Phys. **24**, 053014 (2022).

[17] C. Baumgartner, L. Fuchs, A. Costa, S. Reinhardt, S. Gronin, G. C. Gardner, T. Lindemann, M. J. Manfra, P. E. F. Junior, D. Kochan, J. Fabian, N. Paradiso, and C. Strunk, Supercurrent rectification and magnetochiral effects in symmetric Josephson junctions, Nat. Nanotechnol. **17**, 39 (2022).

[18] D. Y. Vodolazov, A. Yu. Aladyshkin, E. E. Pestov, S. N. Vdovichev, S. S. Ustavshikov, M. Yu. Levichev, A. V. Putilov, P. A. Yunin, A. I. El'kina, N. N. Bukharov, and A. M. Klushin, Peculiar superconducting properties of a thin film superconductor–normal metal bilayer with large ratio of resistivities, Supercond. Sci. Technol. **31**, 115004 (2018).

[19] F. Ando, Y. Miyasaka, T. Li, J. Ishizuka, T. Arakawa, Y. Shiota, T. Moriyama, Y. Yanase, and T. Ono, Observation of superconducting diode effect, Nature (London) **584**, 373 (2020).

[20] B. Turini, S. Salimian, M. Carrega, A. Iorio, E. Strambini, F. Giazotto, V. Zannier, L. Sorba, and S. Heun, Josephson diode effect in high-mobility InSb nanoflags, Nano Lett. **22**, 8502 (2022).

[21] B. Pal, A. Chakraborty, P. K. Sivakumar, M. Davydova, A. K. Gopi, A. K. Pandeya, J. A. Krieger, Y. Zhang, M. Date, S. Ju, N. Yuan, N. B. M. Schroter, L. Fu, and S. S. P. Parkin, Josephson diode effect from Cooper pair momentum in a topological semimetal, Nat. Phys. **18**, 1228 (2022).

[22] A. Sundaresh, J. I. Vayrynen, Y. Lyanda-Geller, and L. P. Rokhinson, Diamagnetic mechanism of critical current nonreciprocity in multilayered superconductors, Nat. Commun. **14**, 1628 (2023).

[23] D. Y. Vodolazov and F. M. Peeters, Superconducting rectifier based on the asymmetric surface barrier effect, Phys. Rev. B **72**, 172508 (2005).

[24] H. M. Greenhouse, Design of planar rectangular microelectronic inductors, IEEE Trans. Parts, Hybrids, Packag. **10**, 101 (1974).

[25] S. Ustavschikov, M. Y. Levichev, I. Y. Pashenkin, N. Gusev, S. Gusev, and D. Y. Vodolazov, Diode effect in a superconducting hybrid Cu/MoN strip with a lateral cut, J. Exp. Theor. Phys. **135**, 226 (2022).

[26] D. Cerbu, V. N. Gladilin, J. Cuppens, J. Fritzsche, J. Tempere, J. T. Devreese, V. V. Moshchalkov, A. V. Silhanek, and J. Van de

Vondel, Vortex ratchet induced by controlled edge roughness, New J. Phys. **15**, 063022 (2013).

[27] K. Ilin, D. Henrich, Y. Luck, Y. Liang, M. Siegel, and D. Yu. Vodolazov, Critical current of Nb, NbN, and TaN thin-film bridges with and without geometrical nonuniformities in a magnetic field, Phys. Rev. B **89**, 184511 (2014).

[28] D. Suri, A. Kamra, T. N. G. Meier, M. Kronseder, W. Belzig, C. H. Back, and C. Strunk, Non-reciprocity of vortex-limited critical current in conventional superconducting micro-bridges, Appl. Phys. Lett. **121**, 102601 (2022).

[29] Y. Hou, F. Nichele, H. Chi, A. Lodesani, Y. Wu, M. F. Ritter, D. Z. Haxell, M. Davydova, S. Ilic, O. Glezakou-Elbert, A. Varambally, F. S. Bergeret, A. Kamra, L. Fu, P. A. Lee, and J. S. Moodera, Ubiquitous Superconducting Diode Effect in Superconductor Thin Films, Phys. Rev. Lett. **131**, 027001 (2023).

[30] N. Satchell, P. M. Shepley, M. C. Rosamond, and G. Burnell, Supercurrent diode effect in thin film Nb tracks, J. Appl. Phys. **133**, 203901 (2023).

[31] L. Bauriedl, Ch. Bauml, L. Fuchs, Ch. Baumgartner, N. Paulik, J. M. Bauer, K.-Q. Lin, J. M. Lupton, T. Taniguchi, K. Watanabe, Ch. Strunk, and N. Paradiso, Supercurrent diode effect and magnetochiral anisotropy in few-layer $NbSe_2$, Nat. Commun. **13**, 4266 (2022).

[32] B. L. T. Plourde, D. J. Van Harlingen, D. Yu. Vodolazov, R. Besseling, M. B. S. Hesselberth, and P. H. Kes, Influence of edge barriers on vortex dynamics in thin weak-pinning superconducting strips, Phys. Rev. B **64**, 014503 (2001).

[33] V. V. Shmidt, The critical current in superconducting films, Sov. Phys. JETP **30**, 1137 (1970).

[34] R. Kawarazaki, R. Iijima, H. Narita, R. Hisatomi, Y. Shiota, T. Moriyama, and T. Ono, Rectification effect of noncentrosymmetric Nb/V/T superconductor, J. Magn. Soc. Jpn. **47**, 133 (2023).

[35] D. Margineda, A. Crippa, E. Strambini, Y. Fukaya, M. T. Mercaldo, M. Cuoco, and F. Giazotto, Sign reversal diode effect in superconducting Dayem nanobridges, arXiv:2306.00193.

[36] S. Ilić and F. S. Bergeret, Theory of the Supercurrent Diode Effect in Rashba Superconductors with Arbitrary Disorder, Phys. Rev. Lett. **128**, 177001 (2022).

[37] H. Bartolf, A. Engel, A. Schilling, K. Ilin, M. Siegel, H.-W. Hubers, and A. Semenov, Current-assisted thermally activated flux liberation in ultrathin nanopatterned NbN superconducting meander structures, Phys. Rev. B **81**, 024502 (2010).

[38] L. N. Bulaevskii, M. J. Graf, C. D. Batista, and V. G. Kogan, Vortex-induced dissipation in narrow current-biased thin-film superconducting strips, Phys. Rev. B **83**, 144526 (2011).

[39] D. Y. Vodolazov, Saddle point states in two-dimensional superconducting films biased near the depairing current, Phys. Rev. B **85**, 174507 (2012).

[40] R. Wakatsuki, Yu Saito, S. Hoshino, Y. M. Itahashi, T. Ideue, M. Ezawa, Y. Iwasa, and N. Nagaosa, Nonreciprocal charge transport in noncentrosymmetric superconductors, Sci. Adv. **3**, e1602390 (2017).

[41] F. Qin, W. Shi, T. Ideue, M. Yoshida, A. Zak, R. Tenne, T. Kikitsu, D. Inoue, D. Hashizume, and Y. Iwasa, Superconductivity in a chiral nanotube, Nat. Commun. **8**, 14465 (2017).

[42] K. Yasuda, H. Yasuda, T. Liang, R. Yoshimi, A. Tsukazaki, K. S. Takahashi, N. Nagaosa, M. Kawasaki, and Y. Tokura, Nonreciprocal charge transport at topological insulator/superconductor interface, Nat. Commun. **10**, 2734 (2019).

[43] K. D. Usadel, Generalized Diffusion Equation for Superconducting Alloys, Phys. Rev. Lett. **25**, 507 (1970).

[44] M. Yu. Kuprianov and V. F. Lukichev, Influence of boundary transparency on the critical current of "dirty" $SS'S$ structures, Sov. Phys. JETP **67**, 1163 (1988).